Spin channels exploring finite superlattices: Vertical and lateral transport

M. de Dios-Leyva,[1] G. E. Marques,[2] and J. C. Drake[1]
[1]*Departamento de Física Teórica, Universidad de La Havana, San Lázaro y L, Vedado 10400, Havana, Cuba*
[2]*Departamento de Física, Universidade Federal de São Carlos, 13560-905 São Carlos, SP, Brazil*
(Received 8 October 2009; published 23 April 2010)

We have investigated spin-dependent transport properties in finite semiconductor superlattices containing N periods. Spin-orbit coupling is taken into account by including the linear Dresselhaus term into the effective Hamiltonian. We have derived analytical expressions for spin-polarized transmission coefficients, density of states, group velocities, and phase delay times for these systems. It is shown that the miniband structure of infinite semiconductor superlattices is spin dependent and plays a fundamental role in the description and understanding of these quantities. For N-period superlattices, these quantities are oscillating functions of the electron energy and their maxima and/or minima are always localized inside the corresponding spin-split minibands. The oscillations disappear for energies inside the superlattice minigaps. We have identified two electron energy ranges where the spin-split minibands do not show overlap and, within these energy ranges, the polarization efficiency is essentially 100%, suggesting that these systems may be explored as possible spin filtering mechanism, even for unpolarized injection from the emitter layer. It is also shown that the energy range where the spin-split resonant minibands show overlap may be also explored as lateral multichannel spin filters, but their efficiencies depend on the degree of resonant peak overlapping.

DOI: 10.1103/PhysRevB.81.155320 PACS number(s): 42.70.Qs, 78.20.Ci, 41.20.Jb

I. INTRODUCTION

The transport of spin-polarized carriers through semiconductor heterostructures has received much attention in the last few years. This interest was motivated by new basic spin properties discovered in these structures and by potential applications in a wide range of spintronic devices such as spin filters,[1] spin detectors, and injectors.[2,3] The spin-orbit interaction (SOI), associated either with bulk inversion asymmetry (BIA) and/or with structural inversion asymmetry (SIA), plays a fundamental role in the study of transport in these semiconductor structures. In particular, the coupling between linear momentum and spin degree of freedom lifts the spin degeneracy and leads to spin-dependent properties that can be explored as transport of classical information as well as spin quantum bits through a nanostructure. The different quantities such as reflection and transmission coefficients, local or extended spin polarization, and tunneling times must be dependent on spin orientation, besides the geometrical and physical dependencies inherent to each semiconductor material used in the nanostructure. The SIA term, controlled by external electric fields, and BIA term, associated with the asymmetry intrinsic to crystalline zincblende materials, can be treated within effective mass[1–10] and transfer matrix frameworks.[7–10] In many cases, when studying the spin-oriented transport properties in heterostructures, the interplay between these two SOI terms must be taken into account. Here, however, we are including the k-linear BIA term only since we will be analyzing transport in symmetric heterostructures for the zero electric field and incidence at low-energy (low k-values) limiting cases, thus effects associated with higher k-order Dressellhaus (BIA) (quadratic and cubic) as well as the k-linear SIA terms can be neglected.[3]

On the other hand, an important research topic in spintronics is the development of efficient spin filters, devices that require some control on the spin orientation. In recent years, spin filters based on simple[1,2,4–6] and multiple-barrier semiconductor structures[11–21] have been investigated. It has been demonstrated that asymmetric[1] and symmetric[2,4–6] simple barriers exhibit tunneling transmission coefficients dependent on the spin polarization. Unfortunately, it was also shown that the spin polarization efficiency is relatively low in these structures. Thus, it has been suggested to use multiple-barrier resonant structures to further enhance the device efficiency. The double-barrier semiconductor heterostructures, in presence and absence of external electric fields, is the most widely studied heterostructure. In these systems, the spin-polarization efficiency may be substantially enhanced and reach, in many cases, values near 100% at the peak positions. Similar results were also reported for triple-barrier tunneling diodes.[21] Therefore, such structures could serve as spin filters or even determine Bell's inequalities for entangled electron spins[22] if the enhanced degree of spin-polarization can be tuned for a range of energy and for some specific spin orientation.

The finite zincblende semiconductor SL may be used also to enhance spin-polarized efficiencies and this becomes possible because: (i) transmission coefficients of these structures exhibit resonant peaks at energies localized inside the minibands of the corresponding infinite superlattice, (ii) these minibands are spin dependent. There have been only a few works on spin-dependent transport in finite semiconductor superlattices,[23,24] which were, basically, devoted to the numerical calculation and discussion of the transmission coefficient and associated resonant energies as functions of the spin orientation and SL parameters. However, the information contained in the total accumulated phase Φ (Ref. 16) of the complex transmission amplitude through the SL structure has not received, up to now, a special attention. Important physical quantities related to the spin-dependent transport of electrons, such as the group velocities and the tunneling delay times can be accessed directly from the knowledge of the phase Φ, and these two quantities determine the dynamic

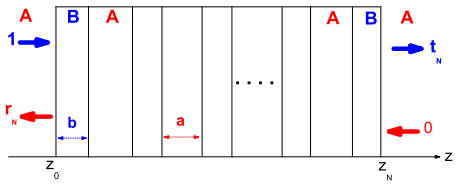

FIG. 1. (Color online) Finite superlattice profile showing the ABABABA semiconductor layer structure, dimensions, and period $d=a+b$. The emitter and collector terminals are assumed to be formed by equal semiconductors. Horizontal arrows indicate the incident, reflected (r_N) and transmitted (t_N) coefficients. For simplicity, the amplitude of incident wave was normalized to one.

working range of a tunneling device. These observations have motivated us to carry out a detailed study of spin-dependent transport of electrons in finite zincblende semiconductor superlattices. In this work we derive analytical expressions for the complex transmission coefficient, total accumulated phase Φ, density of states, group velocities and phase delay times.

The paper is organized as follows. The Sec. II shows details of the theoretical approach and Sec. III is concerned with results and discussion. Finally, our conclusions are given in Sec. IV.

II. THEORETICAL FRAMEWORK

In this work, we will be concerned with spin dependent transport of electrons through a finite superlattice (SL) structure consisting of alternating layers of zincblende semiconductors A and B, periodically distributed along the [001] direction, which is taken as the z axis, as shown qualitatively in Fig. 1. In this SL we define $d=a+b$ as the length or period of the corresponding unit cell, where a and b are the widths of layers A and B, respectively. For simplicity, in what follows we consider the SL as a one-dimensional (1D) symmetric structure formed by rectangular barriers (layers B) and wells (layers A). Also, we suppose that the semiconductors A and B exhibit a relatively strong Dresselhaus spin-orbit interaction. So, within envelope function approximation, the Schrödinger equation for conduction electrons in each layer reads

$$\left\{\left[\frac{\hbar^2(\hat{k}_x^2+\hat{k}_y^2+\hat{k}_z^2)}{2m^*(z)}+V(z)\right]I+\hat{H}_D\right\}F(\vec{r})=EF(\vec{r}), \quad (1)$$

where $m^*(z)$ is the position-dependent electron effective mass, $V(z)$ is the heterostructure potential profile and I is the 2×2 identity matrix. Also, $\hat{H}_D$ is the Dresselhaus SOI Hamiltonian due to the bulk inversion asymmetry in zincblende materials which, for low kinetic energy regime, may be approximated only by the k-linear term[2]

$$\hat{H}_D=\gamma(z)(\sigma_y\hat{k}_y-\sigma_x\hat{k}_x)\hat{k}_z^2, \quad (2)$$

where $\gamma(z)$ represents the z-dependent strength of the spin-orbit (SO) coupling constant, σ_x and σ_y are Pauli spin matrices. As is well known,[7,25] the envelope wave functions describing the dynamics of the electrons through the structure satisfy the boundary conditions

$$\text{(a)}\quad F(\vec{r})\quad \text{and}\quad \text{(b)}\quad v_zF(\vec{r}), \quad (3)$$

must be continuous in any interface. In the presence of SOI, the z-component of the velocity operator becomes

$$\hat{v}_z=\frac{\hbar\hat{k}_z}{m^*(z)}I+\frac{2\gamma(z)}{\hbar}(\sigma_y\hat{k}_y-\sigma_x\hat{k}_x)\hat{k}_z, \quad (4)$$

and these conditions assure the continuity of the probability density and the current density across each boundary. Due to the translational invariance along the xy plane, the wavevector $\vec{k}_p=(k_x,k_y)=(k_p\cos\varphi,k_p\sin\varphi)$ becomes a good quantum number. Thus, the Hamiltonian in Eq. (1) is separable and the spin-polarized eigenfunctions may be chosen as

$$F(\vec{r})=\chi_\pm(\varphi)\exp i(\vec{k}_p\cdot\vec{\rho})u_\pm(k_p,z), \quad (5)$$

where $\vec{\rho}$ is the electron position in the xy plane, and[2] the two-component functions

$$\chi_\pm(\varphi)=\frac{1}{\sqrt{2}}\begin{bmatrix}1\\ \mp\exp(-i\varphi)\end{bmatrix} \quad (6)$$

describe spinor states with well defined values of the spin projection along the polarization vectors $\vec{P}_+=+\vec{\mu}$ and $\vec{P}_-=-\vec{\mu}$, respectively. Here, $\vec{\mu}=(-\cos\varphi,\sin\varphi,0)$ is an in-plane unitary vector and φ denotes the polar angle for the wavevector $\vec{k}_p$ with length $k_p=\sqrt{k_x^2+k_y^2}$.

Furthermore, the functions for the spin-polarized states, $u_\pm(k_p,z)$ shown in Eq. (5), satisfy the eigenvalue problem

$$\left\{\frac{\hbar^2}{2}\hat{k}_z\left[\frac{1}{m_\pm(z,k_p)}\hat{k}_z\right]+V(z)\right\}u_\pm(k_p,z)=E_\pm(k_p)u_\pm(k_p,z), \quad (7)$$

where $E_\pm(k_p)=[E_\pm-\hbar^2k_p^2/2m^*(z)]$ and

$$m_\pm(z,k_p)=m^*(z)[1\pm 2\gamma(z)m^*(z)k_p/\hbar^2]^{-1} \quad (8)$$

are k_p-dependent eigenvalues and SOI renormalized electron effective masses along the z direction of the layers. Within this approach, the spin projections along the vectors $\pm\vec{\mu}$ are conserved.

By applying the velocity operator $\hat{v}_z$ on functions in Eq. (5) and taking into account that the spin operator $(\sigma_y\hat{k}_y-\sigma_x\hat{k}_x)$ is diagonalized[2] by spinors $\chi_\pm(\varphi)\exp i(\vec{k}_p\cdot\vec{\rho})$, we find

$$\hat{v}_zF(\vec{r})=-i\hbar\exp i(\vec{k}_p\cdot\vec{\rho})\chi_\pm(\varphi)\frac{1}{m_\pm(z,k_p)}\frac{du_\pm(k_p,z)}{dz}. \quad (9)$$

Since both $\hat{v}_zF(\vec{r})$ and $F(\vec{r})$ are expressed as products of functions depending separately on spin, $\vec{\rho}$, and z, the continuity shown in Eqs. (3) and (4) reduce to the following boundary conditions for the two-component functions:

$$f_\pm(z,k_p)=\begin{bmatrix}u_\pm(z)\\ \dfrac{1}{m_\pm(z,k_p)}\dfrac{du_\pm(z)}{dz}\end{bmatrix}\quad \text{are continuous.} \quad (10)$$

This result is a direct consequence of the fact that the velocity operator $\hat{v}_z$ has diagonal form in the spinors $\chi_\pm(\varphi)\exp i(\vec{k}_p\cdot\vec{\rho})$. For cases where the velocity operator is

not diagonal, the corresponding spin-dependent boundary conditions[26,27] are, in general, different from Eq. (10).

In order to obtain the transmission coefficients through a finite SL structure [see Fig. 1], it is necessary: (i) to solve Eq. (7) for each spin polarized state and, (ii) by using continuity conditions in Eq. (10) we determine the relation between emitter and in the collector wave functions.

For simplicity of notation, the spin polarization signs ($\pm$) in the above equations will be omitted in the following calculations where we use the transfer matrix method to obtain the transfer matrix W through the SL unit cell, which may be written as (see Appendix)

$$W = \begin{bmatrix} W_{11} & W_{12} \\ W_{21} & W_{22} \end{bmatrix}, \tag{11}$$

where the matrix elements are

$$W_{11} = \cos aQ_1 \cos bQ_2 - \frac{1}{\tau}\sin aQ_1 \sin bQ_2, \tag{12}$$

$$W_{12} = \frac{m_1(k_p)}{Q_1}[\sin aQ_1 \cos bQ_2 + \tau \cos aQ_1 \sin bQ], \tag{13}$$

$$W_{21} = -\frac{Q_1}{m_1(k_p)}\left[\sin aQ_1 \cos bQ_2 + \frac{1}{\tau}\cos aQ_1 \sin bQ_2\right], \tag{14}$$

$$W_{22} = \cos aQ_1 \cos bQ_2 - \tau \sin aQ_1 \sin bQ_2. \tag{15}$$

The other terms in these matrix elements are

$$\tau = \frac{m_2(k_p)}{m_1(k_p)}\frac{Q_1}{Q_2}, \tag{16}$$

$$Q_i = \sqrt{\frac{2m_i^*}{\hbar^2}[E_i(k_p) - V_i]}\left(1 \pm \frac{2m_i^*\gamma_i k_p}{\hbar^2}\right)^{-1/2}, \quad i = 1,2 \tag{17}$$

In these equations, $E_i(k_p)=[E-\hbar^2k_p^2/2m_i^*]$ and the terms m_i^*, $m_i(k_p)$, Q_i, V_i, and γ_i stand for the electron effective mass, spin-dependent effective mass [see Eq. (8)], z component of the wavevector, potential profile and SOI constant of layers A (wells or $i=1$) and B (barriers or $i=2$), respectively.

The transfer matrix through N unit cells and established between the points z_0 in the emitter and z_N in the collector (see Fig. 1), becomes

$$M = W_N W_{N-1} \ldots W_2 W_1 \equiv W^N. \tag{18}$$

By using the Cayley-Hamilton theorem (a matrix obeys its own eigenvalue equation) and the fact that W is a 2×2 unimodular unit cell matrix, it can be demonstrated that $M = W^N$ can be written as[28]

$$M = W^N = \frac{\sin N\beta}{\sin \beta}W - \frac{\sin(N-1)\beta}{\sin \beta}I, \tag{19}$$

where β is the Bloch phase associated with the infinite semiconductor SL ($N\to\infty$) which satisfies the SL dispersion relation

$$\cos \beta = \frac{1}{2}tr(W) = \cos aQ_1 \cos bQ_2 - \frac{1}{2}\left(\tau + \frac{1}{\tau}\right) \times \sin aQ_1 \sin bQ_2 = f(E) \tag{20}$$

Results in Eqs. (18)–(20) show that the unit cell transfer matrix W, the number of unit cells N, and the Bloch phase β associated with the infinite SL play a fundamental role in the study of the spin-dependent transport of electrons through a finite SL structure. As shown in Fig. 1, the total wave function in the emitter side ($z<z_0$) is a linear combination of incoming (incident) and outgoing (reflected) waves in the form

$$u_L(k_p,z) = e^{iQ_{1L}(z-z_0)} + r_N e^{-iQ_{1L}(z-z_0)}. \tag{21}$$

Also, in the collector side ($z>z_N$), the transmitted wave can be written as

$$u_R(k_p,z) = t_N e^{iQ_{1R}(z-z_N)}, \tag{22}$$

where r_N and t_N are the reflection and transmission amplitudes. To obtain the relation between r_N and t_N, it is necessary to use the fact that W^N, in Eq. (19), is the transfer matrix trough N unit cells and the two-component function $f(z,k_p)$ [see Eq. (10)] is continuous at the points z_0 in the emitter and z_N in the collector [see Fig. 1]. This gives

$$\begin{bmatrix} t_N \\ 0 \end{bmatrix} = \hat{T}\begin{bmatrix} 1 \\ r_N \end{bmatrix}, \tag{23}$$

where

$$\hat{T} = \begin{bmatrix} T_{11} & T_{12} \\ T_{21} & T_{22} \end{bmatrix} = S_R^{-1}W^N S_L, \tag{24}$$

is the total transfer matrix, S_L and S_R are left and right side propagation matrices calculated at the left (emitter) and right (collector) interfaces of the SL and given by

$$S_j = \begin{bmatrix} 1 & 1 \\ iQ_{1j}/m_j & -iQ_{1j}/m_j \end{bmatrix}, \quad for \quad j = L,R, \tag{25}$$

and Q_{1j}/m_j, $j=R,L$, are quantities associated with carriers traveling through emitter ($j=L$) or collector ($j=R$) of the SL structure.

Taking into account that W^N is a unimodular matrix, it follows from Eqs. (23)–(25) the transmission amplitude

$$t_N = \frac{\mathrm{Det}(\hat{T})}{T_{22}} = \frac{\mathrm{Det}(S_R^{-1})\mathrm{Det}(S_L)}{T_{22}} = \frac{m_R Q_{1L}}{m_L Q_{1R}}\frac{1}{T_{22}}, \tag{26}$$

where Det stands for determinant.

In the following part we will be focusing our attention on the most common SL structure where emitter and collector regions are made of the same semiconductor as in the well regions (see Fig. 1). In this case, $Q_{1L}/m_L = Q_{1R}/m_R$ and the

complex transmission amplitude may be written as

$$t_N = \frac{1}{T_{22}} = |t_N| e^{i\Phi}, \tag{27}$$

where Φ is the total phase accumulated as the electron propagates through the structure, which is proportional to the total active SL length[28] $D=z_N-z_0$ i. e., $\Phi=Dk_N$, where k_N is the effective propagation wavevector.

After substituting Eq. (19) into Eq. (24) and using the fact that

$$S_R = S_L = S_1 = \begin{bmatrix} 1 & 1 \\ iQ_1/m_1(k_p) & -iQ_1/m_1(k_p) \end{bmatrix}, \tag{28}$$

the total transfer matrix becomes

$$\hat{T} = \frac{\sin N\beta}{\sin \beta} S_1^{-1} W S_1 - \frac{\sin(N-1)\beta}{\sin \beta} I. \tag{29}$$

Thus, using Eqs. (11)–(15) and (28) in the latter equation, the element T_{22} of the total transfer matrix is given by

$$T_{22} = \cos N\beta - i \frac{\sin N\beta}{\sin \beta} G(\omega), \tag{30}$$

where

$$G(\omega) = \frac{1}{2}\left[\frac{Q_1}{m_1(k_p)} W_{12} - \frac{m_1(k_p)}{Q_1} W_{21} \right] = \sin aQ_1 \cos bQ_2 + \frac{1}{2}\left(\tau + \frac{1}{\tau} \right) \cos aQ_1 \sin bQ_2. \tag{31}$$

Furthermore, the function $G(\omega)$ and both $\cos N\beta$ and $\sin N\beta/\sin \beta$ are real quantities because: (i) Q_1 (wells) is always real because $E \geqq V_1$ in these SL layers [see Eq. (17)]; (ii) Q_2 (barriers) will be real for $E \geqq V_2$ and becomes a pure imaginary number otherwise [see also Eq. (17)]; and (iii) the Bloch phase β is real inside the allowed minibands and equal to $i\theta$ or to $\pi+i\theta$ in the energy gap regions, where θ is a real angle. It follows from these results and Eq. (30) that the phase Φ in Eq. (27) satisfies the equation

$$\tan \Phi = \frac{G(\omega) \tan N\beta}{\sin \beta}. \tag{32}$$

Since Eqs. (27), (30)–(32), and (20) completely determine the complex transmission amplitude t_N for each electron spin state, they can be used to study some physical quantities closely related to the spin-dependent transport of electrons through the finite semiconductor SL. In fact, they can be used to calculate the transmission coefficient,

$$T(E) = |t_N|^2 = \frac{1}{|T_{22}|^2}, \tag{33}$$

as well as the density of states $\rho(E)$, the group velocity $v_g(E)$ and the phase delay time[16] τ_{pd} for each spin state, quantities obtained from the accumulated phase $\Phi=Dk_N$ via the equations[28]

$$\text{(a)} \quad \rho(E) = \frac{dk_N}{dE}, \quad \text{(b)} v_g(E) = \frac{dE}{\hbar dk_N}, \quad \text{(c)} \tau_{pd} = \hbar \frac{d\Phi}{dE}. \tag{34}$$

Equations (32) and (20) can be used to determine the analytical expression for $d\Phi/dE$ and, after some algebraic manipulation, we are led to

$$\frac{d\Phi}{dE} = \frac{(1-f^2)\tan N\beta (dG/dE)}{\sqrt{1-f^2}[1+G^2 \tan^2 N\beta - f^2]} - \frac{[N(1+\tan^2 N\beta)\sqrt{1-f^2} - f \tan N\beta] G(df/dE)}{\sqrt{1-f^2}[1+G^2 \tan^2 N\beta - f^2]}. \tag{35}$$

This equation is important since it provides exact expressions for the density of states, group velocity and phase delay time for each spin state orientation in the SL structure.

Before presenting numerical results, let us discuss briefly some aspects of the quantities $T(E)$ and $d\Phi/dE$, which will help the description and understanding of spin-dependent transport properties in finite SL structures. The transmission coefficient T assumes value one for both spin orientations in a SL of N unit cells when $N\beta=Nkd=m\pi$, with $m=1,2,\ldots,(N-1)$ and k being the Bloch wavevector along the z-axis. These conditions are independent of the specific dependence of function $G(\omega)$ [see Eq. (31)] on the unit cell sizes. It is also apparent that T is a periodic function of k with period π/Nd. Thus, when the electron energy E varies within an allowed miniband, $T(E)$ displays oscillations as a function of E and exhibits a resonant structure with resonant energies determined by the corresponding dispersion relations evaluated at $k=m\pi/Nd$. For electron energy inside minigaps, k is a complex quantity and, therefore, the resonant structure of $T(E)$ disappears. Furthermore, $\frac{d\Phi}{dE}$ also exhibits similar structure as $T(E)$, as can be seen in Eq. (35). In general, $\frac{d\Phi}{dE}$ and $T(E)$ exhibit different resonant structures or more specifically, their spectra are slightly different for finite values of N but becomes essentially identical for SL structures with very large periods N.

III. RESULTS AND DISCUSSION

Let us use this analytical description to carry out a detailed study of spin-dependent transport in finite zincblende semiconductor SL. For the numerical calculations we have chosen SL formed by GaSb (wells) and $Al_{0.3}Ga_{0.7}Sb$ (barriers), semiconductors exhibiting very strong Dresselhaus SOI coupling constants. The parameters appropriate for this SL are[2,3] $m_1^*=0.041m_0$, $\gamma_1=187$ eV-Å^3, and $V_1=0$ for GaSb and $m_2^*=0.053m_0$, $\gamma_2=76$ eV-Å^3, and $V_2=0.43$ eV for $Al_{0.3}Ga_{0.7}Sb$. Finally, the zero of energy is taken at the bottom of the conduction band of the *GaSb* layers.

Let us discuss the properties of the miniband structure for an infinite SL as functions of the spin orientation. Figure 2(a) shows the two lowest miniband energy curves, calculated from Eq. (20), for a SL with sizes: $a=60$ Å, $b=30$ Å and plotted as a function of the reduced Bloch wavevector $kd/\pi=\beta/\pi$. Since the Dresselhaus SOI term is proportional

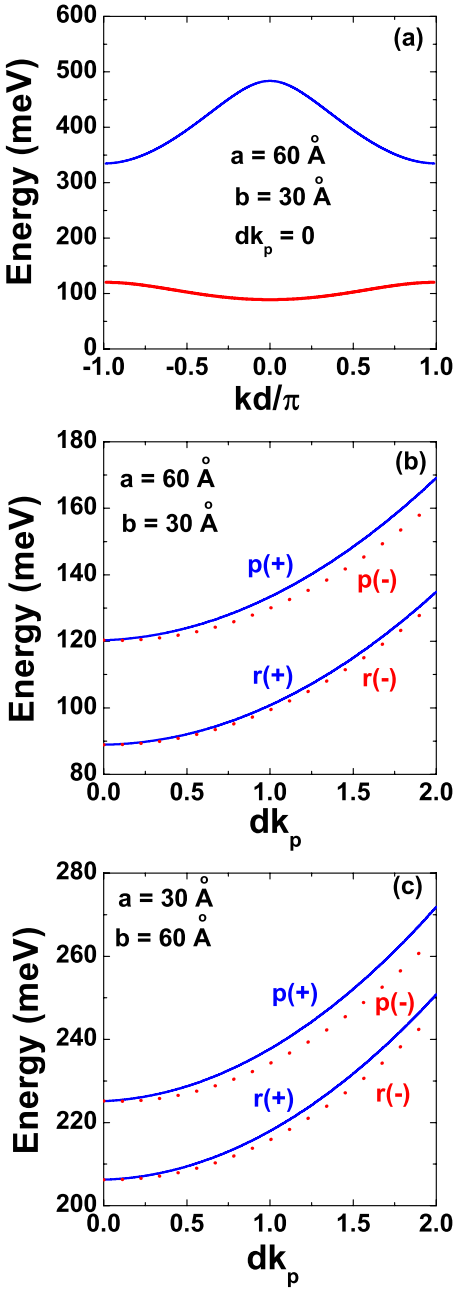

FIG. 2. (Color online) (a) The two lowest dispersion curves for an infinite semiconductor SL composed of alternating layers of GaSb (wells) and $Al_{0.3}Ga_{0.7}Sb$ (barriers), for $a=60$ Å, $b=30$ Å, and $dk_p=0$. The energy is presented as a function of the reduced Bloch wavevector kd/π. Energies corresponding to the band edges of the lowest miniband as functions of dk_p for (b) $a=60$ Å, $b=30$ Å, and (c) $a=30$ Å, $b=60$ Å. Curves $r(+)$ and $r(-)$ [$p(+)$ and $p(-)$] represent the band edges at $k=0[k=\pm\pi/d]$ for spin states χ_+ and χ_-, respectively.

to the in-plane wavevector k_p, the miniband structure only lifts the spin degeneracy for $k_p\neq 0$. The spin split at the miniband edges of the infinite SL with sizes $a=60$ Å, $b=30$ Å is shown as a function of the dimensionless quantity dk_p in Fig. 2(b). The SOI effects associated with larger barrier size is seen in Fig. 2(c), for a SL with sizes $a=30$ Å, $b=60$ Å. Curves labeled $r(+)$ and $r(-)$ [$p(+)$ and $p(-)$] represent the energies of spin states χ_+ and χ_- at $k=0(k=\pm\pi/d)$, respectively, and show that the spin splitting increases with increasing dk_p and quantum confinement in the well regions. It should be emphasized that, for given values of $dk_p\neq 0$, a and b, the spin-splitting miniband for spin up (spin down) is localized in the energy range determined by the corresponding $r(+)$ and $p(+)$ [$r(-)$ and $p(-)$] band edges. Further, the energy ranges for which the spin-splitting minibands do not overlaps are of special interest because they exhibit interesting spin filtering properties, as we will see later. Note that, for given values of $dk_p\neq 0$, a and b, these energy ranges are localized between the $r(+)$ and $r(-)$ band edges and between the $p(+)$ and $p(-)$ band edges. It is clearly seen that the widths of both energy ranges increases with dk_p, as expected.

We now turn to the study of the spin-dependent transmission coefficient spectra and polarization efficiency for finite GaSb−$Al_{0.3}Ga_{0.7}Sb$ semiconductor SLs. The transmission coefficients $T_+(E)$ and $T_-(E)$ associated with spin states χ_+ and χ_-, respectively, are obtained from Eq. (33). The degree of spin polarization can be calculated as

$$P(E)=\frac{T_+(E)-T_-(E)}{T_+(E)+T_-(E)}. \tag{36}$$

It should be pointed out that we are only considering spin effects in energy ranges inside the lowest spin splitting minibands of the corresponding infinite SL. The spin polarized transmission coefficients and the degree of spin polarization at $dk_p=0,2$, for finite SL with increasing numbers of unit cells N, are presented in the sequence of figures (Figs. 3–7) but keeping the same two periods of the infinite SLs shown in Figs. 2(b) and 2(c). The energy dependence with $N=2$ (double barrier diodes) are displayed in Figs. 3 and 4, respectively. At same SOI strength, $dk_p=2$, the spin splitting of transmission peaks increases with the quantum confinement and this increase makes the polarization efficiency at the resonant energy slightly lower in Fig. 3(c) ($a=60$ Å, and $b=30$ Å) than in Fig. 4(c) ($a=30$ Å, and $b=60$ Å). A comparison between Figs. 2(b) and 3 and between Figs. 2(c) and 4 reveals that the resonant energies associated with transmission peaks are always localized inside the lowest spin-split miniband of the infinite SL. For instance, the peak for spin-up (spin-down) close to 150 meV (145 meV) in Fig. 3(b) is localized within the allowed miniband situated between the $r(+)$ and $p(+)$ [$r(-)$ and $p(-)$] band edges shown in Fig. 2(b), for $dk_p=2$. Similarly, the resonance energy ($E\approx 112$ meV) associated with the degenerate peak shown in Fig. 3(a) is situated inside the corresponding miniband at $dk_p=0$ [see Fig. 2(b)].

Furthermore, since we are dealing with exact calculations, the spin polarized transmission peak exhibit value $T=1$ for each spin state. In general, the finite SL containing N unit cells displays $(N-1)$ spin degenerate transmission peak structure in the absence of SOI ($dk_p=0$), which splits into $2(N-1)$ resonant peaks in the presence of SOI ($dk_p\neq 0$). Certainly, when the number of unit cells (N) increases, the spin polarized resonant peaks of the transmission coefficient ($T=1$) occur at much closer energy values which are distributed inside the sharp miniband broadening of the infinite SL.

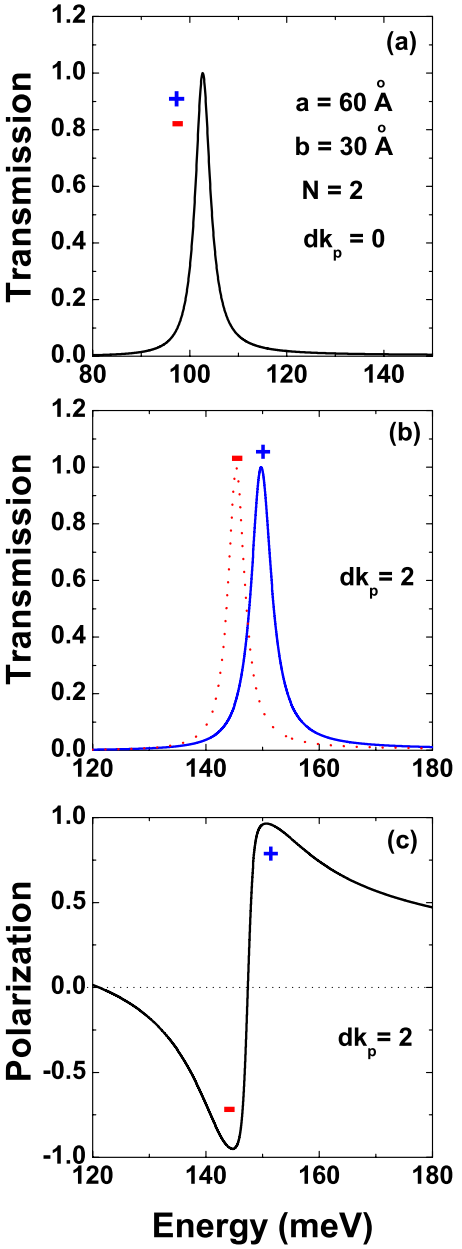

FIG. 3. (Color online) Transmission coefficient and polarization efficiency as functions of the energy for a double-barrier resonant device ($N=2$) with $a=60$ Å, $b=30$ Å, and $dk_p=0,2$. Signs + and − correspond to spin-up and spin-down states or χ_+ and χ_-, respectively.

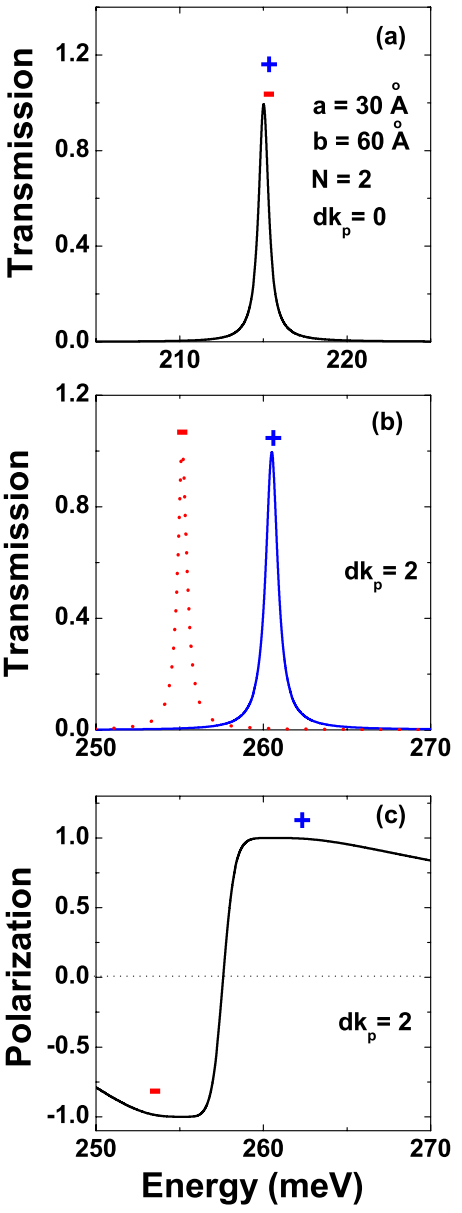

FIG. 4. (Color online) The same as Fig. 3, but interchanging the dimensions: $a=30$ Å and $b=60$ Å.

Therefore, the energy separation between spin-split peaks decreases, the overlap between them may increase which leads to smaller degree of spin polarization away from the resonant peak energy. It is noted that resonant lines of $T(E)$ at same SOI strength, as depicted in Fig. 6(b) for $a=30$ Å, are narrower than in Fig. 5(b) for $a=60$ Å, and this result may be assigned to quantum confinement effects.

The resonant energies localized inside the spin-split miniband are determined by the dispersion relation evaluated at the Bloch wavevectors $k_m=m\pi/Nd$, with $m=1,2,\ldots,(N-1)$. For SLs with sufficiently large number of periods N, there will have a certain number of k_m vectors near the center and the edges of the Brillouin zone. As a consequence, a number of spin-polarized resonant peaks will be displaced to lower and higher energy ranges. Some of these transmission peaks on the left (spin-down) and on the right (spin-up) will show no overlap, as can be seen on left and right sides of Figs. 5(b), 6, and 7(b). These isolated spin polarized transmission corresponds essentially to 100% polarization efficiency and, therefore, this finite SL can be explored as possible vertical spin filtering mechanism, even for unpolarized injection at the emitter. Inside the energy range where the spin-split minibands show overlapping, the polarization efficiency $P(E)$ becomes an oscillating function of the incident electron energy and the peak values of $P(E)$ depend on the degree of overlapping between the adjacent transmission coefficients $T_+(E)$ and $T_-(E)$. Anyhow, for specially designed finite SL, these peaks may also be explored as a longitudinal

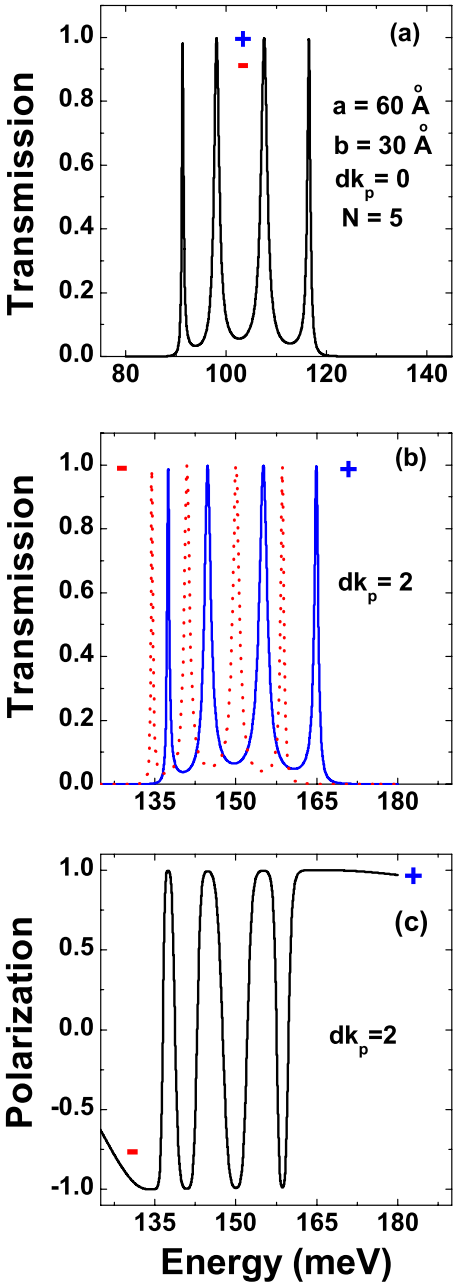

FIG. 5. (Color online) The same as in Fig. 3, but for $N=5$. Observe in panel (b) the spin-up and spin-down isolated resonant peaks with energies close to 165 meV and 134 meV, respectively.

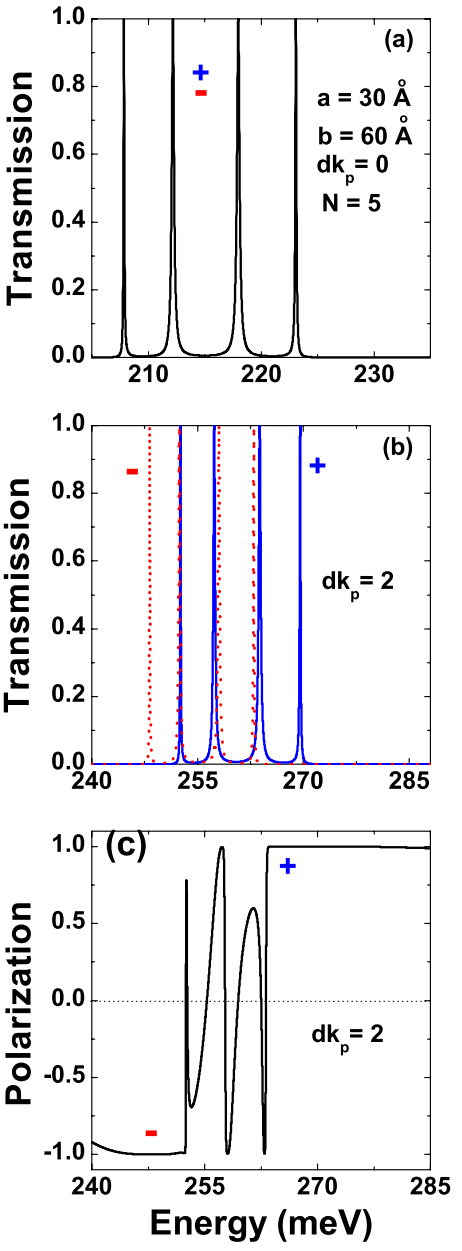

FIG. 6. (Color online) The same as in Fig. 5, but with interchanged sizes $a=30$ Å and $b=60$ Å. Observe in panel (b) the spin-up (spin-down) isolated resonant peaks with energy above (below) 265 (255) meV.

multichannel spin filter, foreseeing technological progresses in the near future for the construction of efficient spin-selecting detectors not only on the collector side of the finite SL (vertical transport) but also as source and drain contacts near to left and right interfaces in order to explore spin-polarized longitudinal transport along the well layers.

Certainly, any technical possibility to explorer these structures as spin filtering devices requires some knowledge on spin-dependent group velocity v_g and phase delay time τ_{pd}, quantities which provide valuable information about the dynamical ranges for finite SLs. The delay time may be understood as due to repeated Bloch reflections of electron in the structure before it manages to escape the localization region. In order to better appreciate these results, we display in Figs. 8–10 both quantities as functions of incident electron energy, for the same SL parameters used in Figs. 3–6, respectively. The group velocity v_g is depicted in units of $v_0=1.52\times10^7 d$ (Å) cm/s, where d(Å) is the length of the SL unit cell in Å. For each spin state and SL configuration, the energy dependence of $\tau_{pd}(E)$ exhibits maxima and minima at energies where the group velocity $v_g(E)$ takes its minimum and maximum values, respectively [see also Eq. (34)]. The resonant energy spectra for $\tau_{pd}(E)$ and transmission coefficient $T(E)$ are essentially identical, thus, when a resonant transmission occurs, the phase delay time and group velocity take, approximately, their corresponding maximum and mini-

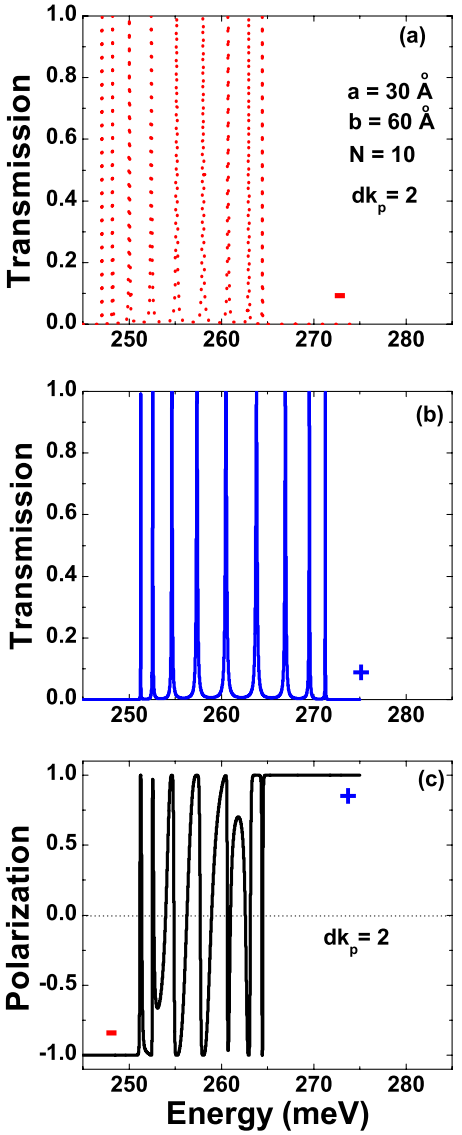

FIG. 7. (Color online) Transmission coefficient and polarization efficiency as functions of the energy for $a=30$ Å, $b=60$ Å, $N=10$, and $dk_p=2$. Panels (a) and (b) show results for spin states χ_+ and χ_-, respectively. Observe in these two panels the set of spin-up (spin-down) isolated resonant peaks with energy above (below) 265 (250) meV.

mum values, respectively. Effects associated to SOI splits each degenerate peak of τ_{pd} at $dk_p=0$ into two peaks when $dk_p \neq 0$ and the lower energy state (χ_-) stays much longer times inside the well layers before tunneling and this is understood as due to quantum confinement effect and to the higher tunnel barrier seen for this lower energy carrier. Finally, observe in Figs. 9(b) and 2(b) [Figs. 10(b) and 2(c)] that two peaks of $\tau_{pd}(E)$ are located in the energy ranges where the spin-splitting minibands do not overlap. More specifically, these peaks, localized at $E \approx 134$ meV and 164 meV [$E \approx 248$ meV and 270 meV], correspond to different spin states and the time localization for the first is several times larger than for the other. Interesting enough, these finite SLs may show dynamic spin filtering properties in energy ranges substantially different and specially designed structures corroborates their exploration as filtering devices.

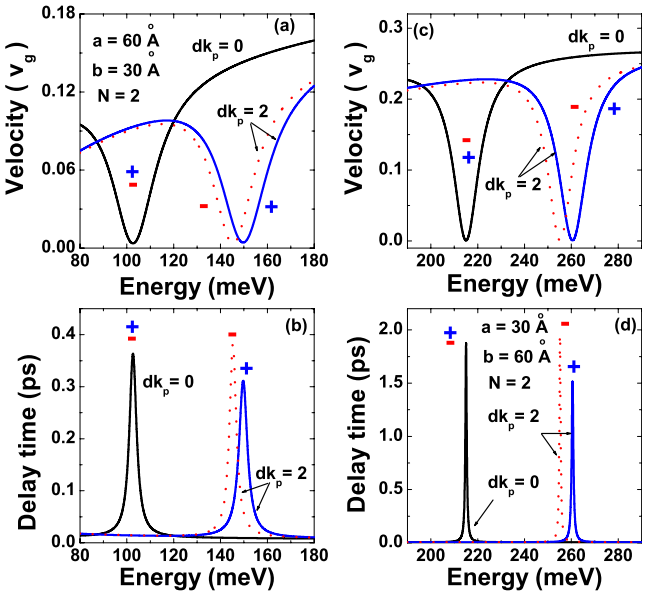

FIG. 8. (Color online) Group velocity and phase delay time as functions of the energy for a double-barrier resonant device ($N=2$) with $dk_p=0,2$; $a=60$ Å and $b=30$ Å [panels (a) and (b)], and $a=30$ Å, $b=60$ Å [panels (c) and (d)]. Signs + and − correspond to spin states χ_+ and χ_-, respectively.

IV. CONCLUSIONS

We have carried out a detailed study of spin-dependent transport properties in finite zincblende semiconductor SLs containing N periods $d=a+b$. The Dresselhaus spin-orbit coupling taken into account in the effective Hamiltonian is responsible for spin-splitting. With the help of the transfer-matrix method, we have derived analytical expressions for the complex transmission coefficients, which allowed the calculation of dynamical properties such as density of states, group velocity and phase delay time. We have shown that the spin-dependent miniband structure of infinite semiconductor SLs plays a fundamental role in the description and in understanding of the properties associated with these dynamical quantities. Specifically, these quantities are oscillating functions of the electron energy for a N-period SL and their maxima and/or minima are always localized inside the corresponding spin-split miniband. These oscillations disappear for energies inside the SL minigaps. We have identified two electron energy ranges were transmission energy peaks and spin-split minibands do not overlap. In these energy ranges, the polarization efficiency is essentially 100%, suggesting that the finite SL system may be explored as vertical spin filtering mechanisms even for unpolarized injection. Finally, inside the energy ranges where the spin-split minibands overlap, they may be also explored as longitudinal multichannel spin filters, but their efficiencies depend on the degree of resonant peak overlapping. We stress that these results and analysis can be readily extended in order to treat other finite N-period semiconductor SL using particular semiconductors where the inclusion of the Rashba term may predominates.

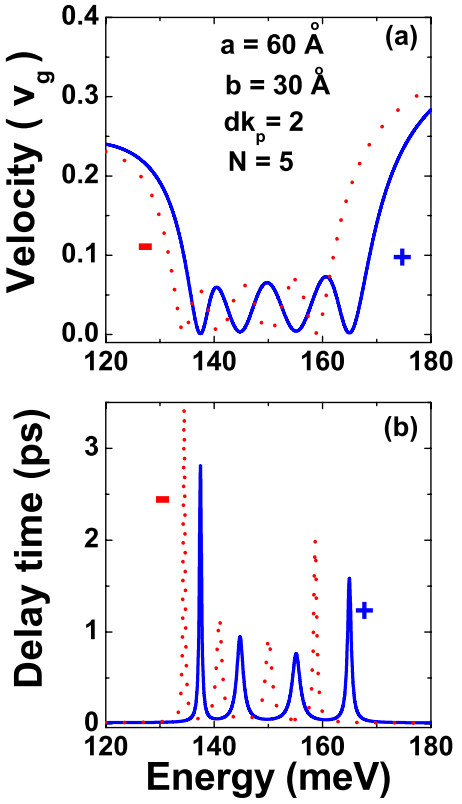

FIG. 9. (Color online) Group velocity (v_g) and phase delay time (τ_{pd}) as functions of the energy for $N=5$; $dk_p=2$; and $a=60$ Å, $b=30$ Å. Signs + and − correspond to spin states χ_+ and χ_-, respectively.

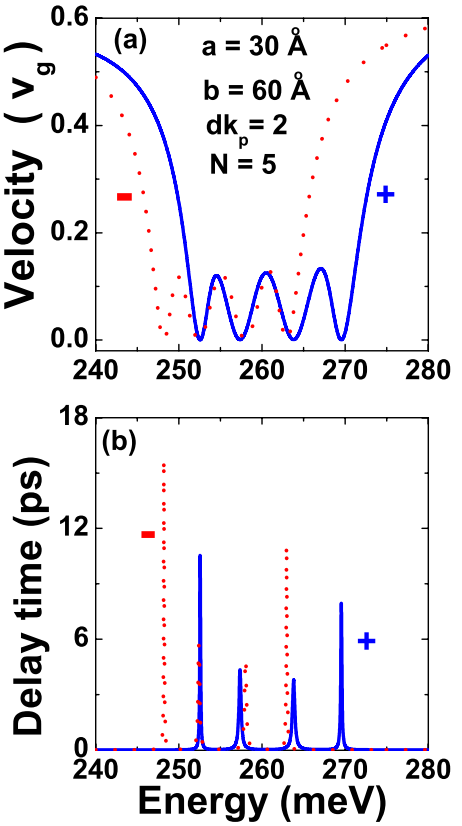

FIG. 10. (Color online) Group velocity (v_g) and phase delay time (τ_{pd}) as functions of the energy for $N=5$; $dk_p=2$; and $a=30$ Å, $b=60$ Å. Signs + and − correspond to spin states χ_+ and χ_-, respectively.

ACKNOWLEDGMENTS

The authors are grateful for the financial support provided by the Brazilian agencies FAPESP and CNPq and by the Alma Mater Project of the University of Havana.

APPENDIX

To derive expressions in Eqs. (12)–(17), it should be noted that the general solution of Eq. (7) for $u(k_p,z)$ in each layer may be written as

$$u(k_p,z) = A_0 \cos[Q(z-z_a)] + B_0 \frac{m(k_p)}{Q} \sin[Q(z-z_a)], \tag{37}$$

where A_0 and B_0 are constants, z_a denotes an arbitrary point in each of the layer materials, and $m(k_p)$ and Q are defined in Eqs. (8) and (17), respectively. Since the transfer matrix (unimodular) in each layer may be written as

$$M(z-z_a) = \begin{bmatrix} \cos[Q(z-z_a)] & \frac{m(k_p)}{Q}\sin[Q(z-z_a)] \\ -\frac{Q}{m(k_p)}\sin[Q(z-z_a)] & \cos[Q(z-z_a)] \end{bmatrix}, \tag{38}$$

the two-component function $f(z,k_p)$ [see Eq. (10)] associated with the solution (37) can be written in the form

$$f(z,k_p) = M(z-z_a) f(z_a,k_p). \tag{39}$$

Using this equation and the continuity for $f(z,k_p)$, one can easily arrive to the expression

$$W = M_A(a) M_B(b), \tag{40}$$

for the transfer matrix W defined in Eq. (11), where

$$M_A(a) = \begin{bmatrix} \cos aQ_1 & \frac{m_1(k_p)}{Q_1}\sin aQ_1 \\ -\frac{Q_1}{m_1(k_p)}\sin aQ_1 & \cos aQ_1 \end{bmatrix}, \tag{41}$$

$$M_B(b) = \begin{bmatrix} \cos bQ_2 & \frac{m_2(k_p)}{Q_2}\sin bQ_2 \\ -\frac{Q_2}{m_2(k_p)}\sin bQ_2 & \cos bQ_2 \end{bmatrix}, \tag{42}$$

are the transfer matrices through layers A and B, respectively. It is easy to verify that the matrix elements of W, shown in Eq. (40), are as the definition in Eqs. (12)–(15).

[1] A. Voskoboynikov, S. S. Liu, and C. P. Lee, Phys. Rev. B **58**, 15397 (1998).
[2] V. I. Perel, S. A. Tarasenko, I. N. Yassievich, S. D. Ganichev, V. V. Bel'kov, and W. Prettl, Phys. Rev. B **67**, 201304(R) (2003).
[3] P. S. Alekseev, V. M. Chistyakov, and I. N. Yassievich, Semiconductors **40**, 1402 (2006).
[4] L. G. Wang, W. Yang, K. Chang, and K. S. Chan, Phys. Rev. B **72**, 153314 (2005).
[5] V. A. Sablikov and Y. Ya. Tkach, Phys. Rev. B **76**, 245321 (2007).
[6] T. Fujita, M. B. A. Jalil, and S. G. Tan, J. Phys.: Condens. Matter **20**, 115206 (2008).
[7] A. C. Rodrigues Bittencourt, A. M. Cohen, and G. E. Marques, Phys. Rev. B **57**, 4525 (1998).
[8] E. A. de Andrada e Silva and G. C. La Rocca, Phys. Rev. B **59**, R15583 (1999).
[9] H. B. de Carvalho, M. J. S. P. Brasil, V. López-Richard, Y. Galvão Gobato, G. E. Marques, I. Camps, L. C. O. Dacal, M. Henini, L. Eaves, and G. Hill, Phys. Rev. B **74**, 041305(R) (2006).
[10] C. F. Destefani, S. E. Ulloa, and G. E. Marques, Phys. Rev. B **70**, 205315 (2004).
[11] A. Voskoboynikov, S. S. Liu, and C. P. Lee, Phys. Rev. B **59**, 12514 (1999).
[12] G. E. Marques, A. C. R. Bittencourt, C. F. Destefani, and S. E. Ulloa, Phys. Rev. B **72**, 045313 (2005).
[13] David Z.-Y. Ting and X. Cartoixa, Phys. Rev. B **68**, 235320 (2003).
[14] K. Gnanasekar and K. Navaneethakrishnan, Physica E **28**, 328 (2005).
[15] K. Gnanasekar and K. Navaneethakrishnan, Phys. Lett. A **341**, 495 (2005).
[16] L. Yu and O. Voskoboynikov, J. Appl. Phys. **98**, 023716 (2005).
[17] R. Romo and S. E. Ulloa, Phys. Rev. B **72**, 121305(R) (2005).
[18] W. Li and Y. Guo, Phys. Rev. B **73**, 205311 (2006).
[19] J. Gong, X. X. Liang, and S. L. Ban, J. Appl. Phys. **102**, 073718 (2007).
[20] A. J. Peter, Phys. Lett. A **372**, 5239 (2008).
[21] T. Koga, J. Nitta, H. Takayanagi, and S. Datta, Phys. Rev. Lett. **88**, 126601 (2002).
[22] D. S. Saraga and D. Loss, Phys. Rev. Lett. **90**, 166803 (2003).
[23] C. Moyses Araújo, A. Ferreira da Silva, and E. A. de Andrada e Silva, Phys. Rev. B **65**, 235305 (2002).
[24] Ch.-Z. Ye, R. Xue, Y.-H. Nie, and J.-Q. Liang, Phys. Lett. A **373**, 1290 (2009).
[25] Calvin Yi-Ping Chao and S. L. Chuang, Phys. Rev. B **43**, 7027 (1991).
[26] U. Zülicke and C. Schroll, Phys. Rev. Lett. **88**, 029701 (2001).
[27] L. W. Molenkamp, G. Schmidt, and G. E. W. Bauer, Phys. Rev. B **64**, 121202(R) (2001).
[28] J. M. Bendickson, J. P. Dowling, and M. Scalora, Phys. Rev. E **53**, 4107 (1996).